Journal of Molecular Cell Biology (2023), 15(9), mjad060 https://doi.org/10.1093/jmcb/mjad060
Published online September 28, 2023

Article

Targeting hepatic ceruloplasmin mitigates nonalcoholic steatohepatitis by modulating bile acid metabolism

Quanxin Jiang†, Ning Wang†, Sijia Lu†, Jie Xiong, Yanmei Yuan*, Junli Liu*, and Suzhen Chen*

Shanghai Diabetes Institute, Department of Endocrinology and Metabolism, Shanghai Sixth People's Hospital Affiliated to Shanghai Jiao Tong University School of Medicine, Shanghai 200233, China
† These authors contributed equally to this work.
* Correspondence to: Yanmei Yuan, E-mail: yuanyanmei727@126.com; Junli Liu, E-mail: liujunli@sjtu.edu.cn; Suzhen Chen, E-mail: cszdream@163.com

Edited by Feng Liu

Nonalcoholic steatohepatitis (NASH) is a condition that progresses from nonalcoholic fatty liver disease (NAFLD) and is characterized by hepatic fat accumulation, inflammation, and fibrosis. It has the potential to develop into cirrhosis and liver cancer, and currently no effective pharmacological treatment is available. In this study, we investigate the therapeutic potential of targeting ceruloplasmin (Cp), a copper-containing protein predominantly secreted by hepatocytes, for treating NASH. Our result show that hepatic Cp is remarkedly upregulated in individuals with NASH and the mouse NASH model. Hepatocyte-specific Cp ablation effectively attenuates the onset of dietary-induced NASH by decreasing lipid accumulation, curbing inflammation, mitigating fibrosis, and ameliorating liver damage. By employing transcriptomics and metabolomics approaches, we have discovered that hepatic deletion of Cp brings about remarkable restoration of bile acid (BA) metabolism during NASH. Hepatic deletion of Cp effectively remodels BA metabolism by upregulating Cyp7a1 and Cyp8b1, which subsequently leads to enhanced BA synthesis and notable alterations in BA profiles. In conclusion, our studies elucidate the crucial involvement of Cp in NASH, highlighting its significance as a promising therapeutic target for the treatment of this disease.

Keywords: ceruloplasmin, nonalcoholic steatohepatitis, bile acid, inflammation, fibrosis

Introduction

Nonalcoholic steatohepatitis (NASH) is a liver disease characterized by the presence of fat accumulation and severe inflammation within the liver, which can ultimately lead to damage of hepatocytes. Furthermore, the condition may worsen by the deposition of collagen fibers within the liver, exacerbating the severity of the disease. NASH is a progressive form of nonalcoholic fatty liver disease (NAFLD) and represents a critical stage in the progression to fibrosis and cirrhosis of the liver (Michelotti et al., 2013; Sheka et al., 2020; Loomba et al., 2021; Huby and Gautier, 2022). The occurrence of NASH increases the risk of liver cirrhosis and liver cancer, resulting in an elevated incidence and mortality rate (Michelotti et al., 2013). Globally, the prevalence of NAFLD exceeds 25% and is rapidly increasing, with an estimation of 10%–59% of patients progressing to the NASH stage (Goh and McCullough, 2016; Younossi et al., 2016, 2018; Zhou et al., 2020). Currently, the treatment options for NASH are limited, as there are no approved pharmacotherapies to combat this prevalent medical condition (Harrison et al., 2023). Therefore, it is imperative to conduct further research to pinpoint the key molecular regulators responsible for the advancement and escalation of NASH, thus facilitating the development of effective therapeutic options for its treatment.

Ceruloplasmin (Cp), as a copper-containing liver secretory protein, plays a crucial role in maintaining copper balance within the body by binding to ∼90% of copper ions in the plasma and controlling their distribution (Linder, 2016; Samygina et al., 2017; Blades et al., 2021). Cp also possesses antioxidant properties and acts as an oxidase, facilitating the oxidation reactions of polyphenols and polyamines. Furthermore, Cp exhibits

Received July 16, 2023. Revised September 19, 2023. Accepted September 27, 2023.

ferroxidase activity, which is essential for the metabolism of iron elements (Harris, 2000; Blades et al., 2021). Cp is closely associated with metabolic disorders, as demonstrated by clinical studies revealing elevated levels of Cp in the patients afflicted with metabolic syndrome, diabetes, and cardiovascular diseases (Mänttäri et al., 1994; Kim et al., 2002; Engstrom et al., 2003). Our previous findings showed that liver-specific knockout of Cp in mice leads to ameliorated NAFLD by reducing hepatic steatosis and enhancing mitochondrial function (Xie et al., 2022). This signals potential therapeutic targets for NAFLD by restoring copper homeostasis and adenosine monophosphate-activated protein kinase (AMPK) activation. Cp acts as an acute-phase reactant protein and its plasma concentration increases in response to inflammation, trauma, tissue damage, or infection (Vasilyev, 2010). Moreover, Cp serves as a regulator of copper and iron metabolism (Roeser et al., 1970; Gulec and Collins, 2014). Recent research suggests a link between the metabolic processes of copper and iron within the body and the development of inflammation and fibrosis (Hubscher, 2003; Aigner et al., 2010; Preziosi et al., 2017; Flemming, 2023). Hence, it is plausible that Cp potentially contributes to the progression of liver inflammation and fibrosis, either through a direct regulation or by influencing copper and iron metabolism. However, the role of Cp in inflammation and fibrosis in relation to NASH remains inconclusive without definitive research.

With the development of metabolomics, the role of various small-molecule metabolites in the occurrence and progression of metabolic diseases has attracted increasing attention. Bile acids (BAs) are a class of biologically active molecules with multiple functions (Jiao et al., 2022). They are primarily synthesized in the liver and released into the intestine by the gallbladder, where they participate in the metabolism and absorption of nutrients through their emulsification effect. Primary BAs synthesized in the liver are further converted into secondary BAs by the gut microbiota (Chiang, 2004; Wahlstrom et al., 2016). Primary and secondary BAs in the intestine can then be directly transported back to the liver through the enterohepatic circulation via the portal vein, serving as important signaling molecules involved in metabolic regulation within the body (de Aguiar Vallim et al., 2013). Endogenous BAs undergo changes under various physiological, pathological, or therapeutic conditions, and these changes may further drive the occurrence of related metabolic abnormalities. Numerous studies have shown that alterations in serum BA levels and composition have close association with several diseases such as obesity, diabetes, NAFLD, and coronary artery atherosclerotic heart disease (Brandl et al., 2018; Fiorucci et al., 2021; Masoodi et al., 2021; Cortes and Eckel, 2022). Meanwhile, BA analogs are also employed in the treatment of NASH. Currently, the only medication demonstrating significant efficacy and showing promise as the first approved candidate compound for NASH treatment is obeticholic acid (OCA) (Eslam et al., 2019; Younossi et al., 2019). OCA is a semi-synthetic derivative of BA and functions as an effective and selective farnesoid X receptor (FXR) agonist. It can alleviate hepatic fat accumulation, inflammation, and fibrosis. However, OCA may induce side effects such as lipid abnormalities and dose-dependent pruritus. Given that NASH is a chronic disease requiring long-term medication, there is a higher demand for the safety of drugs and patient compliance. Therefore, further research is still needed to identify new targets for NASH treatment and develop safer and more effective medications. The interaction between Cp and BAs may serve as a potential therapeutic target. Both Cp and BAs are synthesized in hepatocytes and can be excreted through the bile duct. Hepatocytes utilize cytochrome P450 enzymes (CYPs) to mediate cholesterol oxidation and synthesize primary BAs (Pikuleva, 2006). CYPs are a superfamily of enzymes that contain the heme cofactor, which is a coordinated complex containing an iron ion (Meunier et al., 2004). Cp possesses ferroxidase activity, which can oxidize Fe^{2+} to Fe^{3+} (Harris, 2000; Blades et al., 2021). The synthesis, secretion, and metabolism of BAs and Cp can all respond to changes in the nutritional status of the body. Therefore, there may exist mutual regulatory interactions between BAs and Cp.

In this study, we investigated the therapeutic potential of hepatic Cp deficiency in a high-fat with methionine and choline-deficient diet (HFMCD)-induced mouse NASH model. By transcriptomic and metabolomic analyses, we revealed a novel mechanism involving the modulation of BA metabolism by Cp in regulating NASH.

Results

Hepatic Cp levels are positively associated with NASH

Given that overnutrition has been shown to cause an upregulation of Cp during the development of NAFLD induced by high-fat diet (HFD) (Xie et al., 2022), we investigated the relationship between Cp and NASH. Consistent with our previous findings, *CP* levels were increased in individuals with NAFL (Figure 1A). More significantly, the level of *CP* was markedly higher in individuals with NASH compared to those with NAFL or in the normal group (Figure 1A). Consistently, we observed a profound upregulation of hepatic CP protein level in individuals with NASH (Figure 1B and C). We also observed a noteworthy rise in the levels of Cp expression in the livers and serum from mice with NASH induced by HFMCD compared to that from non-NASH control mice (Figure 1D–G). Furthermore, the level of *Cp* in primary hepatocytes was significantly upregulated by the treatment with palmitic acid (PA) (Figure 1H), which acts as an inducer of NASH *in vitro* (Zhang et al., 2018). The expression of Cp in primary hepatocytes was also significantly upregulated with increasing durations of PA treatment (Figure 1I–K). Thus, an increase in Cp expression may be associated with the progression of NASH. We retrieved high-throughput sequencing datasets from the Gene Expression Omnibus database (GEO) and found a significantly higher *CP* expression level in individuals with NASH compared to those with NAFL (GSE167523; Figure 1L). Similarly, in a NASH mouse model induced by a diet rich in fat, fructose, and cholesterol (FFC), *Cp* exhibited significantly higher expression compared to those fed chow diet (GSE164084; Figure 1M). In an *in vitro* liver system model constructed by human

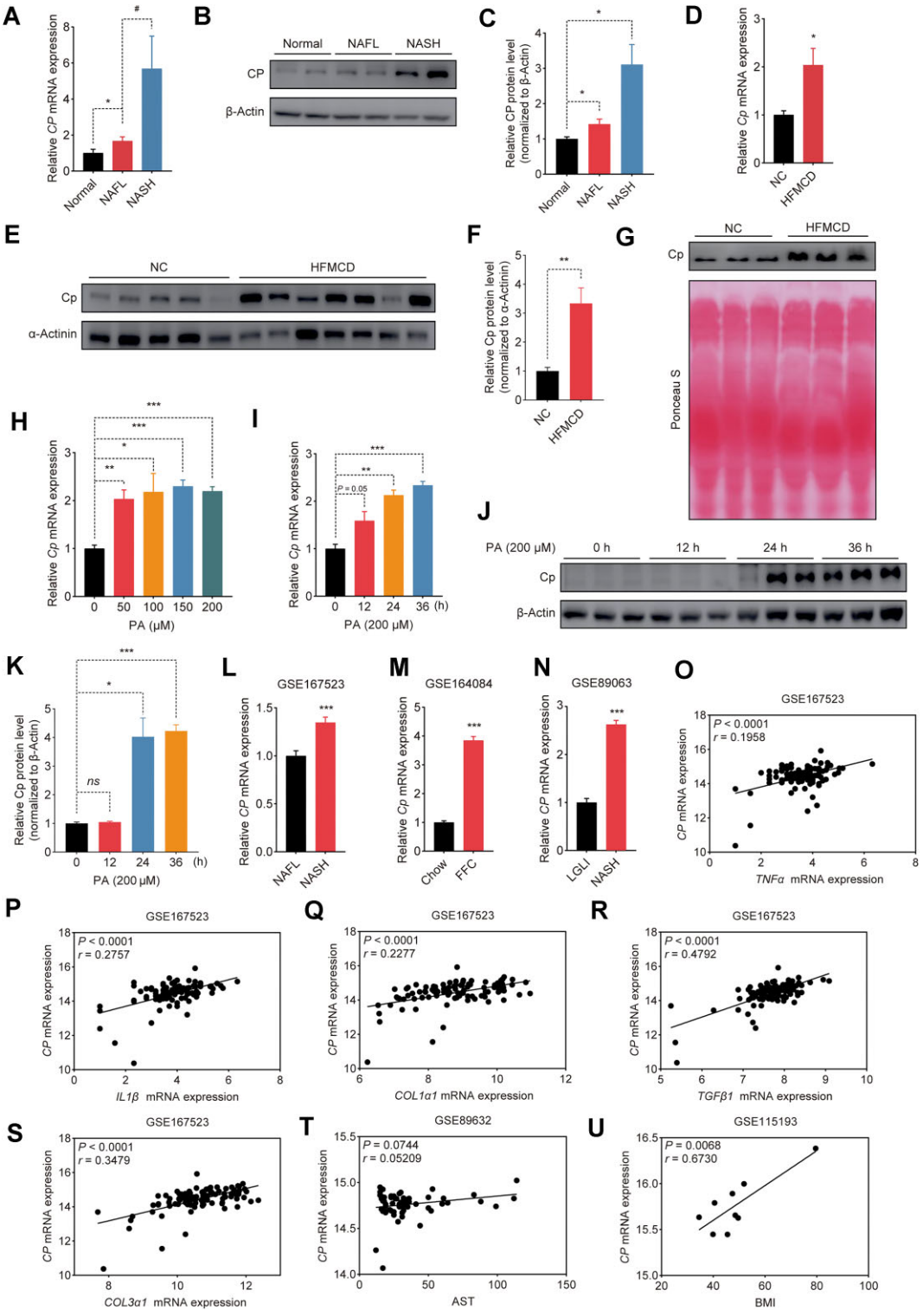

Figure 1 Hepatic Cp levels are positively associated with NASH. (**A**–**C**) qRT-PCR analysis of *CP* mRNA level (**A**) and immunoblot (**B**) with quantitative analysis (**C**) of CP protein level in the livers from individuals with NAFL ($n = 17$), individuals with NASH ($n = 12$), or healthy controls ($n = 14$). (**D**–**F**) qRT-PCR analysis of *Cp* mRNA level (**D**) and immunoblot (**E**) with quantitative analysis (**F**) of Cp protein level in the livers from mice fed normal chow diet (NC) or HFMCD for 8 weeks ($n = 5$). (**G**) Immunoblot analysis of Cp protein level in the serum from mice with NC or HFMCD feeding. (**H**) qRT-PCR analysis of *Cp* mRNA level in the primary hepatocytes treated with PA at various concentrations.

hepatocytes, *CP* showed higher expression under NASH-inducing condition compared to the control group treated with low glucose and low insulin (LGLI) (GSE89063; Figure 1N). Further analysis of the GSE167523 dataset revealed significant positive correlations between *CP* and inflammation-related genes *TNFα* (Figure 1O) and *IL1β* (Figure 1P) and fibrosis-related genes including *COL1α1* (Figure 1Q), *TGFβ1* (Figure 1R), and *COL3α1* (Figure 1S). In two additional human NASH datasets, *CP* also showed positive correlations with aspartate aminotransferase (AST) level (GSE89632; Figure 1T) and body mass index (BMI) (GSE115193; Figure 1U). Collectively, these findings suggest a positive correlation between Cp expression and the progression of NASH.

Hepatocyte-specific Cp deficiency ameliorates HFMCD-induced NASH

To determine the functional role of Cp in NASH development, we generated liver-specific Cp knockout (Cp^{LKO}) mice by crossing $Cp^{flox/flox}$ mice with Alb-cre mice and fed Cp^{LKO} mice and their littermate controls ($Cp^{flox/flox}$) with HFMCD for 8 weeks. Notably, Cp^{LKO} mice exhibited smaller liver size (Figure 2A) and weight (Figure 2B), as well as a lower ratio of liver weight to body weight (Figure 2C), compared to $Cp^{flox/flox}$ mice, despite both groups had similar body weights (Figure 2D). Next, we conducted a histological analysis of the liver tissue using hematoxylin and eosin (H&E) staining. Cp^{LKO} mice exhibited less lipid accumulation (Figure 2E) and lower NAS score (Figure 2F). Consistently, Cp^{LKO} mice showed significantly lower serum triglyceride (TG) (Figure 2G), total cholesterol (TC) (Figure 2H), and hepatic non-esterified fatty acid (NEFA) (Figure 2J) levels and a decreasing trend in serum NEFA level (Figure 2I) compared to $Cp^{flox/flox}$ mice. In addition, we performed an immunohistochemical (IHC) analysis to evaluate the impact of Cp ablation on the inflammatory response, which is another hallmark of NASH. Cp^{LKO} mice showed smaller amount of Tnfα in the liver, indicating a reduction in inflammatory infiltration (Figure 2K and L). Additionally, Cp^{LKO} mice showed significantly lower levels of serum biomarkers for liver injury, such as alanine aminotransferase (ALT) and AST, and lower AST-to-ALT ratio (Sorbi et al., 1999; Kew, 2000; Gu et al., 2023) compared to the control group (Figure 2M–O). Histological analysis of Masson and Sirius Red demonstrated that the hepatic fibrosis deposition was ameliorated in Cp^{KLO} mice (Figure 2P–R). Thus, liver-specific Cp ablation mitigates the progression of NASH.

Cp deficiency suppresses genes linked to hepatic steatosis, inflammation, and fibrosis

To further delve into the influence of liver-specific Cp knockout on NASH progression, we examined the mRNA levels of genes involved in lipid metabolism, inflammatory response, and fibrogenesis. The expression levels of genes involved in fatty acid β-oxidation (FAO) in the liver, including *Pparα*, *Cpt1α*, *Acadm*, and *Hmgcs2*, were significantly higher in Cp^{KLO} mice (Figure 3A). Consistently, the protein levels of Pparα and Cpt1α were enhanced in the livers from Cp^{LKO} mice in comparison to $Cp^{flox/flox}$ mice (Figure 3B and C). However, the mRNA levels of genes related to lipid synthesis or fatty acid uptake did not significantly change (Figure 3D). These results were consistent with our previous report that Cp ablation enhances the level of FAO to alleviate the progression of NAFLD (Xie et al., 2022). Furthermore, enzyme-linked immunosorbent assay (ELISA) demonstrated significantly lower serum Tnfα level in Cp^{LKO} mice than in $Cp^{flox/flox}$ mice (Figure 3E). The mRNA levels of pro-inflammatory markers associated with NASH (Figure 3F) and fibrotic genes (Figure 3G) were also noticeably lower in the livers from Cp^{LKO} mice. These results indicate that hepatic ablation of Cp can alleviate lipid accumulation, inflammatory response, and liver fibrosis in response to HFMCD feeding.

The lessening of inflammation and fibrosis likely results from the alleviation of liver steatosis by Cp deficiency

To investigate the direct effect of hepatic Cp deficiency on lipid accumulation *in vitro*, primary hepatocytes from Cp^{LKO} mice and $Cp^{flox/flox}$ mice were extracted and subjected to PA exposure. Nile Red staining results showed a significant reduction in PA-induced lipid droplet accumulation in hepatocytes lacking Cp compared to the control group (Figure 4A). Moreover, quantitative real-time polymerase chain reaction (qRT-PCR) analysis revealed an obvious upregulation of genes related to FAO in hepatocytes with Cp deficiency (Figure 4B), while mRNA levels of genes associated with fatty acid uptake and synthesis remained unchanged (Figure 4C). To assess how Cp deficiency affects inflammation and fibrosis in the liver, we next extracted hepatic parenchymal cells (HPCs) and non-parenchymal cells (NPCs) from the livers of $Cp^{flox/flox}$ and Cp^{LKO} mice fed HFMCD for a duration of 8 weeks. In line with the findings in cultured primary hepatocytes, a significant upregulation of FAO-related gene expression was observed exclusively in HPCs, but not NPCs, of Cp^{LKO} mice (Figure 4D), while notable downregulation

Figure 1 *(Continued)* (**I**–**K**) qRT-PCR analysis of *Cp* mRNA level (**I**) and immunoblot (**J**) with quantitative analysis (**K**) of Cp protein level in the primary hepatocytes treated with PA (200 μM) for the indicated periods. (**L**) *CP* mRNA level in the livers from individuals with NAFL ($n = 51$) or NASH ($n = 47$) (GSE167523). (**M**) *Cp* mRNA level in the livers from mice fed chow diet or FFC diet (GSE164084; $n = 3$/group). (**N**) *CP* mRNA level in human hepatocytes incubated with LGLI ($n = 9$) or NASH-inducing ($n = 8$) medium (GSE89063). (**O**–**S**) Linear regression analysis of *CP* mRNA level with *TNFα* (**O**), *IL1β* (**P**), *COL1α1* (**Q**), *TGFβ1* (**R**), or *COL3α1* (**S**) mRNA level in high-throughput sequencing data (GSE167523) of human liver tissues ($n = 98$). Each gene expression value was transformed into log2 (transcript expression value plus one). (**T**) Linear regression analysis of *CP* mRNA level with AST in microarray data (GSE89632) of human liver tissues ($n = 63$). (**U**) Linear regression analysis of *CP* mRNA level with BMI in microarray data (GSE115193) of human liver tissues ($n = 9$). The results are presented as mean ± SEM. $^{*}P < 0.05$, $^{**}P < 0.01$, $^{***}P < 0.001$, $^{\#}P < 0.05$. *CP* mRNA levels in individuals with NASH and GSE167523 were analyzed by Mann–Whitney *U* test; other data were analyzed by two-tailed, unpaired Student's *t*-test or with Welch correction.

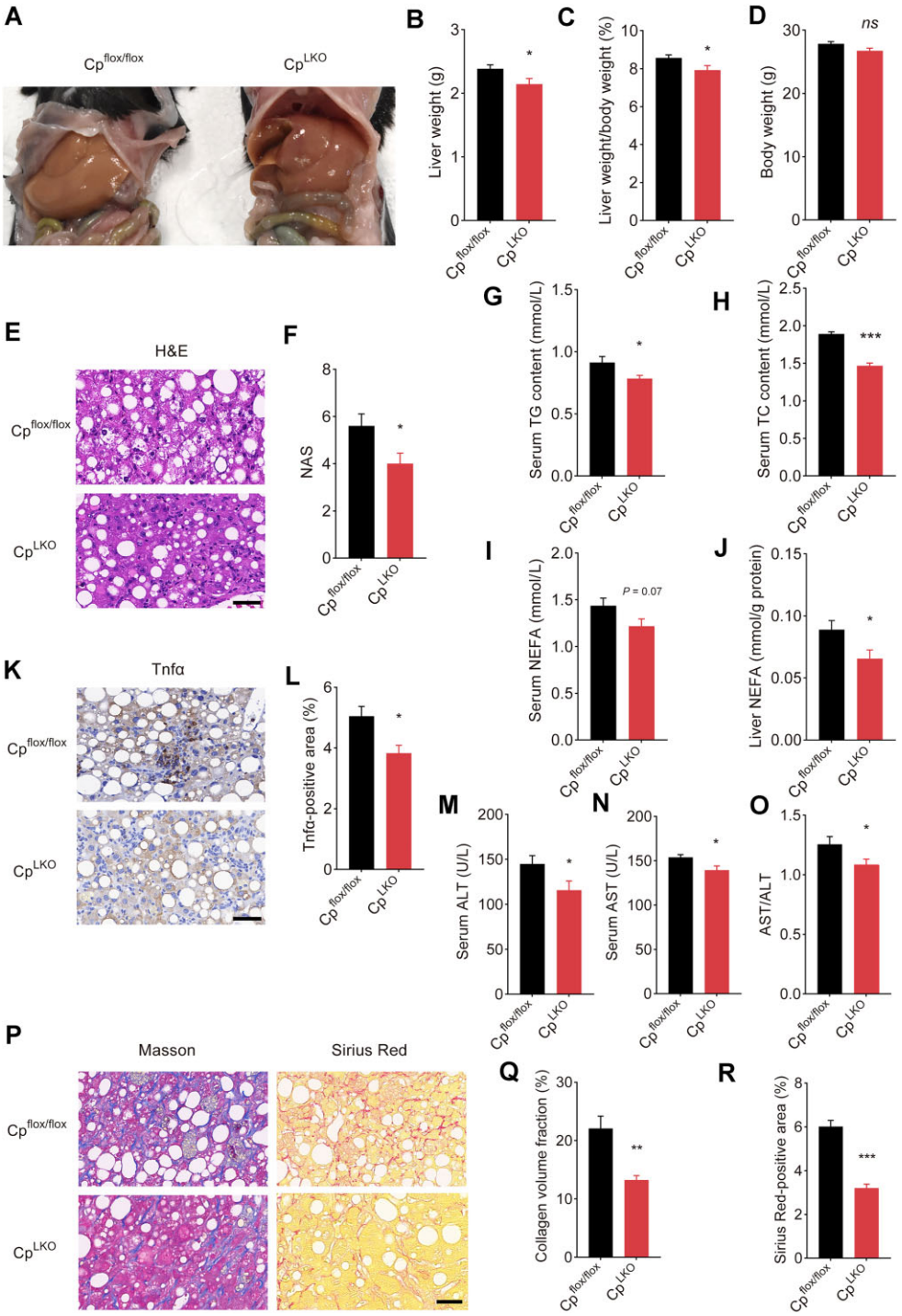

Figure 2 Hepatocyte-specific Cp deficiency ameliorates HFMCD-induced NASH. (**A**) Representative photograph of the livers from $Cp^{flox/flox}$ and Cp^{LKO} mice fed HFMCD for 8 weeks. (**B**–**D**) Liver weight (**B**), liver weight-to-body weight ratio (**C**), and body weight (**D**) of $Cp^{flox/flox}$ mice ($n = 8$) or Cp^{LKO} mice ($n = 10$). (**E** and **F**) H&E histology (**E**) with NAS quantitative analysis (**F**). Scale bar, 50 μm. NAS score represents the sum of scores for steatosis, hepatocellular ballooning, and lobular inflammation. (**G**–**J**) Serum TG (**G**), TC (**H**), and NEFA (**I**) levels and liver NEFA content in the mice ($n = 8$/group). (**K** and **L**) IHC (**K**) with quantitative analysis (**L**) of Tnfα in the livers from $Cp^{flox/flox}$ mice or Cp^{LKO} mice. (**M**–**O**) Serum ALT (**M**) and AST (**N**) levels and AST-to-ALT ratio (**O**) in $Cp^{flox/flox}$ mice or Cp^{LKO} mice ($n = 10$/group). (**P**–**R**) Masson's trichrome staining and Sirius Red staining (**P**) with quantitative analysis for collagen volume (**Q**) and Sirius Red-stained area (**R**). Scale bar, 50 μm. The results are presented as mean ± SEM. $^*P < 0.05$, $^{**}P < 0.01$, $^{***}P < 0.001$. *ns* denotes non-significant. Data were analyzed by two-tailed, unpaired Student's *t*-test or with Welch correction.

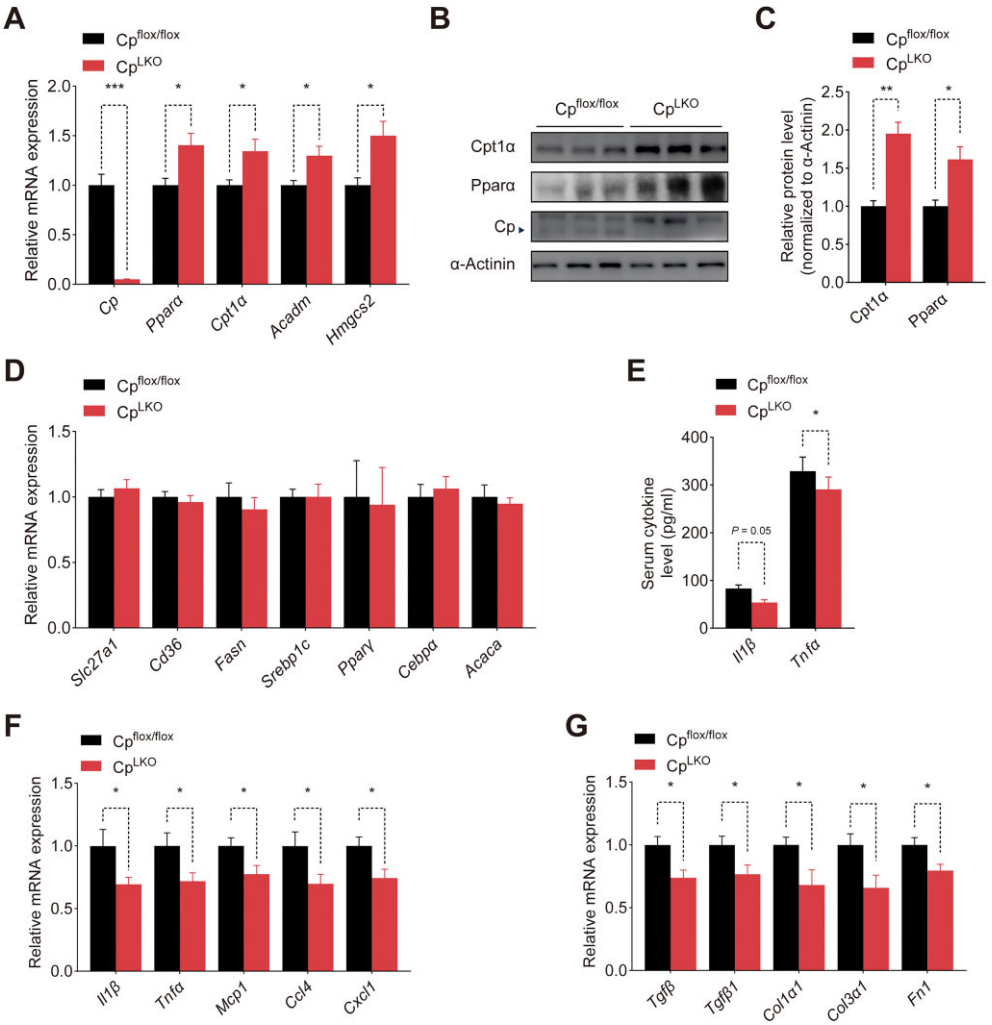

Figure 3 Cp deficiency suppresses genes related to hepatic steatosis, inflammation, and fibrosis. $Cp^{flox/flox}$ and Cp^{LKO} mice were fed HFMCD for 8 weeks. (**A**, **D**, **F**, and **G**) qRT-PCR analysis of FAO-related genes (**A**), lipogenesis-related genes (**D**), pro-inflammatory genes (**F**), and pro-fibrotic genes (**G**) in the livers. (**B** and **C**) Immunoblot (**B**) with quantitative analysis (**C**) of Cpt1α and Pparα protein levels in the livers. (**E**) Serum pro-inflammatory cytokine levels. The results are presented as mean ± SEM. $*P < 0.05$, $**P < 0.01$, $***P < 0.001$. *Ccl4* and *Fn1* mRNA levels in the livers were analyzed by Mann–Whitney *U* test; other data were analyzed by two-tailed, unpaired Student's *t*-test or with Welch correction.

of pro-inflammatory and pro-fibrotic gene expression was found solely in the NPCs, but not HPCs, of Cp^{LKO} mice (Figure 4E and F). These findings suggest that Cp^{LKO} mice exhibit distinct cellular responses depending on the cell type. The enhanced FAO in HPCs potentially ameliorates liver steatosis, which subsequently reduces inflammation and fibrosis. The *in vitro* results further support the *in vivo* observations that a deficiency in Cp can effectively alleviate hepatic steatosis caused by HFMCD, and the improvement in inflammation and fibrosis is most likely due to the amelioration of liver steatosis.

Transcriptomic analysis uncovers the promotion of BA metabolism by Cp deficiency

To deepen our understanding of the molecular mechanisms underlying the therapeutic effects of Cp deletion on NASH in mice, we conducted transcriptomic analysis with the RNA sequencing (RNA-seq) data of liver tissues from HFD-fed mice treated with adenoviruses expressing short hairpin RNA of Cp (AdshCp) or the control shRNA targeting LacZ (AdshLacZ). Principal component analysis (PCA) unveiled a distinct demarcation between the two groups (Figure 5A). A comprehensive analysis of differential expression highlighted a total of 1566 genes that exhibited significant changes in expression levels upon Cp ablation, with 560 genes showing significant upregulation and 1006 genes displaying significant downregulation (Figure 5B). The heatmap depicting differentially expressed genes (DEGs) related to pro-inflammatory and pro-fibrotic processes provided further evidence of Cp ablation in attenuating hepatic inflammation and fibrosis during NASH (Figure 5C). Moreover, we conducted Reactome pathway enrichment (RPE) analysis to further investigate the upregulated DEGs and found a significant enrichment of genes associated with CYPs and BA metabolism (Figure 5D),

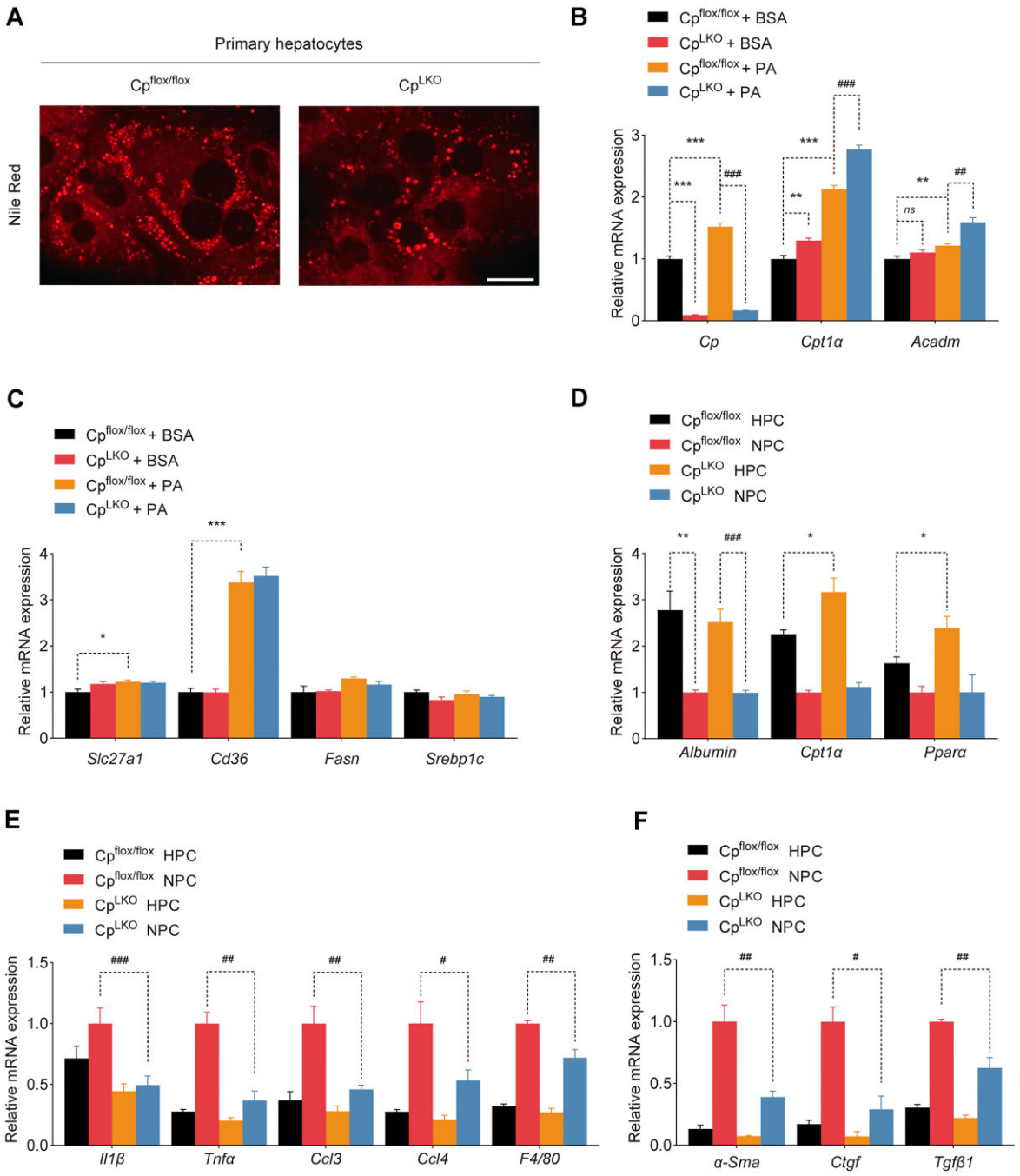

Figure 4 The lessening of inflammation and fibrosis likely results from the alleviation of liver steatosis by Cp deficiency. (**A**–**C**) Primary hepatocytes isolated from $Cp^{flox/flox}$ or Cp^{LKO} mice were treated as indicated. (**A**) Representative images of Nile Red staining after 48 h PA treatment. Scale bar, 20 μm. (**B** and **C**) qRT-PCR analysis of genes related to FAO (**B**) and fatty acid uptake and synthesis (**C**) after treatment with PA or BSA for 24 h. (**D**–**F**) qRT-PCR analysis of FAO-related (**D**), pro-inflammatory (**E**), and pro-fibrotic (**F**) genes in HPCs and NPCs isolated from Cp^{LKO} or $Cp^{flox/flox}$ mice with HFMCD feeding. The results are presented as mean ± SEM. $^{*}P < 0.05$, $^{**}P < 0.01$, $^{***}P < 0.001$, $^{\#}P < 0.05$, $^{\#\#}P < 0.01$, $^{\#\#\#}P < 0.001$. *ns* denotes non-significant. *Ctgf* mRNA level in NPCs was analyzed by Mann–Whitney *U* test; other data were analyzed by two-tailed, unpaired Student's *t*-test or with Welch correction.

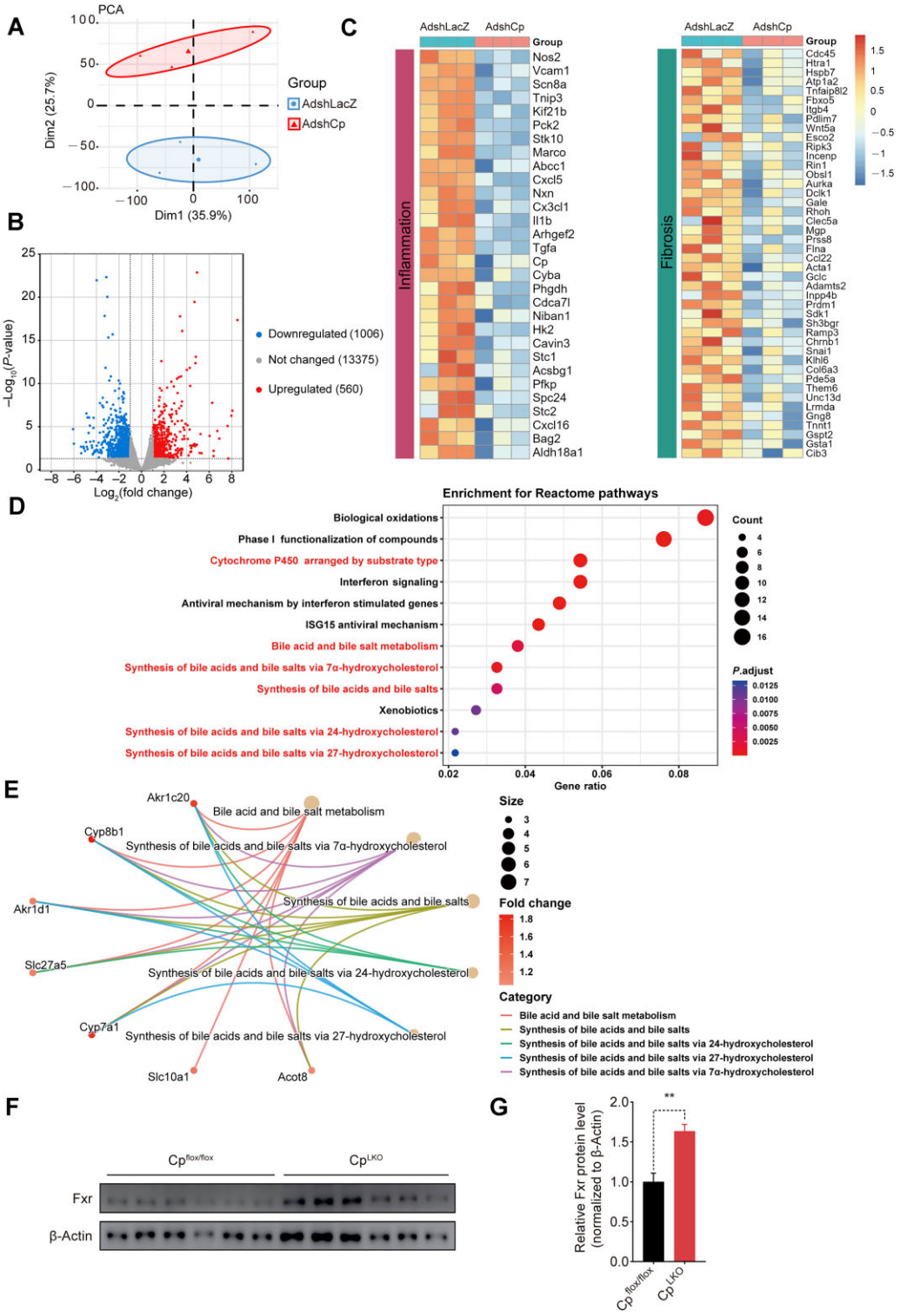

Figure 5 Transcriptomic analysis uncovers the promotion of BA metabolism by Cp deficiency. (**A**–**E**) RNA-seq was performed with three biological replicates per sample of the livers from HFD-fed mice injected with AdshLacZ or AdshCp ($n = 5$/group). (**A**) PCA plot of gene expression data. (**B**) Volcano plot of DEGs (>2-fold, $P < 0.05$). (**C**) Expression profile of genes related to inflammation and fibrosis based on RNA-seq data. (**D**) Reactome pathways enriched in the upregulated DEGs. (**E**) Regulatory network of BA metabolism-related genes determined by the RPE analysis. (**F** and **G**) Immunoblot (**F**) with quantitative analysis (**G**) of Fxr protein levels in the livers from Cp^{LKO} or $Cp^{flox/flox}$ mice with HFMCD feeding. The results are presented as mean ± SEM. $^{**}P < 0.01$. Data were analyzed by two-tailed, unpaired Student's *t*-test.

including key genes involved in hepatic BA synthesis and reabsorption, such as *Cyp7a1*, *Cyp8b1*, *Akr1c20*, *Akr1d1*, *Slc27a5*, *Acot8*, and *Slc10a1* (Figure 5E). In accordance with our previous report that *in vivo* knockdown of Cp can activate the FXR signaling pathway (Xie et al., 2022), we observed a noticeable increase in hepatic Fxr protein level in Cp^{LKO} mice (Figure 5F and G). FXR is a critical regulator of BA metabolism and its upregulation in the absence of Cp may have significant implications during NASH. Therefore, these findings indicate that Cp deficiency potentially exerts its regulatory function by modulating BA metabolism.

Hepatic Cp deficiency leads to alterations in hepatic BA biosynthesis and composition

We next determined the liver enzymes involved in the synthesis of BAs in Cp^{LKO} mice fed HFMCD. The mRNA levels of hepatic *Cyp7a1* and *Cyp8b1* were elevated in Cp^{LKO} mice (Figure 6A), in line with the RNA-seq data. The elevation of *Cyp7a1* and *Cyp8b1* mRNA levels was significant in Cp^{LKO} mice fed HFD (Figure 6B), albeit with a slight variation in mice fed normal chow diet (Figure 6C). The protein expression of Cyp8b1 was also markedly increased (Figure 6D). To gain a deeper understanding of how Cp ablation affects BAs to improve NASH in mice, we conducted metabolomic analysis on BAs within the liver of Cp^{LKO} mice and their controls ($Cp^{flox/flox}$). Orthogonal partial least-square discriminant analysis (OPLS-DA) demonstrated distinct compositions of BAs in the livers of Cp^{LKO} mice and $Cp^{flox/flox}$ mice fed normal chow diet (Figure 6E). Cyp7a1 is the first and the rate-limiting enzyme in the classical BA synthesis pathway and catalyzes the conversion of cholesterol to 7-α-hydroxycholesterol (Wahlstrom et al., 2016). Cp^{LKO} mice exhibited a higher level of total BAs in the liver, consistent with the higher *Cyp7a1* mRNA level (Figure 6F). The concentration percentages of various BA groups in Cp^{LKO} mice were not significantly different from that in $Cp^{flox/flox}$ mice (Figure 6G). The concentration of the 12OH BA species, including deoxycholic acid (DCA), increased (Figure 6H), in line with the higher *Cyp7a1* and *Cyp8b1* mRNA levels in Cp^{LKO} mice. However, the elevated concentrations of non-12OH BAs, including 6-ketolithocholic acid (6-ketoLCA), β-ursodeoxycholic acid (β-UDCA), and taurochenodeoxycholic acid (TCDCA) (Figure 6H), suggested the activation of alternative BA synthesis pathway mediated by Cyp27a1 and Cyp7b1 enzymes. Surprisingly, gene expression levels of *Cyp27a1* and *Cyp7b1* remained largely unaffected. Therefore, we hypothesized that the increased concentrations of non-12OH BAs might be a result of their reabsorption by hepatocytes.

Hepatic-specific knockout of Cp remodels serum BA profiles

To decipher the underlying molecular mechanism of the altered BA profiles in the liver, we assessed serum BA profiles in Cp^{LKO} and $Cp^{flox/flox}$ mice fed normal chow diet, using ultra-performance liquid chromatography coupled with triple-quadrupole mass spectrometry (UPLC/TQ-MS). PLS-DA score plot demonstrated distinct clusters of serum BAs in Cp^{LKO} mice and $Cp^{flox/flox}$ mice (Figure 7A). Both the heatmap and bar plots clearly demonstrated significant fluctuations between the serum BA profiles of Cp^{LKO} mice and $Cp^{flox/flox}$ mice (Figure 7B–D). The concentrations of unconjugated BAs, including both unconjugated 12OH BAs and unconjugated non-12OH BAs, were significantly reduced in the Cp^{LKO} group (Figure 7E). The percentages of unconjugated BAs in the serum closely mirrored the concentration alterations (Figure 7F). At the distal end of the ileum, the majority of unconjugated BAs are reabsorbed into intestinal cells through sodium-dependent BA transporter and transported into the portal circulation via basolateral BA transporters (OSTα, OSTβ, and MRP2) (Tveter et al., 2023). Cp knockout reduced the levels of unconjugated BAs in the serum but did not affect that in the liver, suggesting that Cp knockout may affect the reabsorption of unconjugated BAs in the intestine. Besides, the percentages of conjugated BAs, especially conjugated non-12OH BAs, were significantly higher in the Cp^{LKO} group (Figure 7F). The concentrations of unconjugated non-12OH BAs, including 12-ketolithocholic acid (12-ketoLCA), ursocholic acid (UCA), α-muricholic acid (αMCA), murocholic acid (muroCA), and β-muricholic acid (βMCA), and unconjugated 12OH BAs, including 3-ketocholic acid (3-ketoCA) and allocholic acid (ACA), were significantly reduced in Cp^{LKO} mice (Figure 7G). The upregulated expression of BA synthesis-related liver enzymes and the reduced concentrations of unconjugated BAs in Cp^{LKO} mice imply that Cp may influence NASH progression through altering BA metabolism pathways.

Discussion

Hepatokines are essential in the development of metabolic disorders and play a critical role in the pathogenesis of NASH (Kim et al., 2021; Montgomery et al., 2022; Stefan et al., 2023). An in-depth comprehension of the involvement of hepatokines in hepatic steatosis and dysfunction can lead to better strategies for NASH prevention and treatment. Cp is a copper-containing secretory protein mainly synthesized in the liver. In this study, we demonstrated the therapeutic potential of target ablation of Cp for treating steatohepatitis and elucidated the underlying mechanism involving BA metabolism. Mice with Cp depletion in hepatocytes exhibited resistance to HFMCD-induced steatosis, inflammation, fibrosis, and liver damage. Mechanistically, we found that Cp depletion in the liver upregulated the expression levels of *Cyp7a1* and *Cyp8b1*, the key enzymes in the classical pathway of BA synthesis, and altered the composition of BAs in the liver and serum, thereby alleviating NASH. Thus, hepatic Cp represents a promising therapeutic target for NASH treatment.

Liver lipid overload causes severe damage to the liver, including hepatocellular injury, inflammation, and fibrosis (Marra and Svegliati-Baroni, 2018). The liver serves as an important copper ion reservoir, and Cp regulates the homeostasis of copper ions in the liver. Increasing evidence suggests that imbalances in hepatic copper levels contribute to various metabolic disorders (Tang et al., 2000; Harder et al., 2022). We previously demonstrated that in a mouse model of NAFLD, Cp knockout can

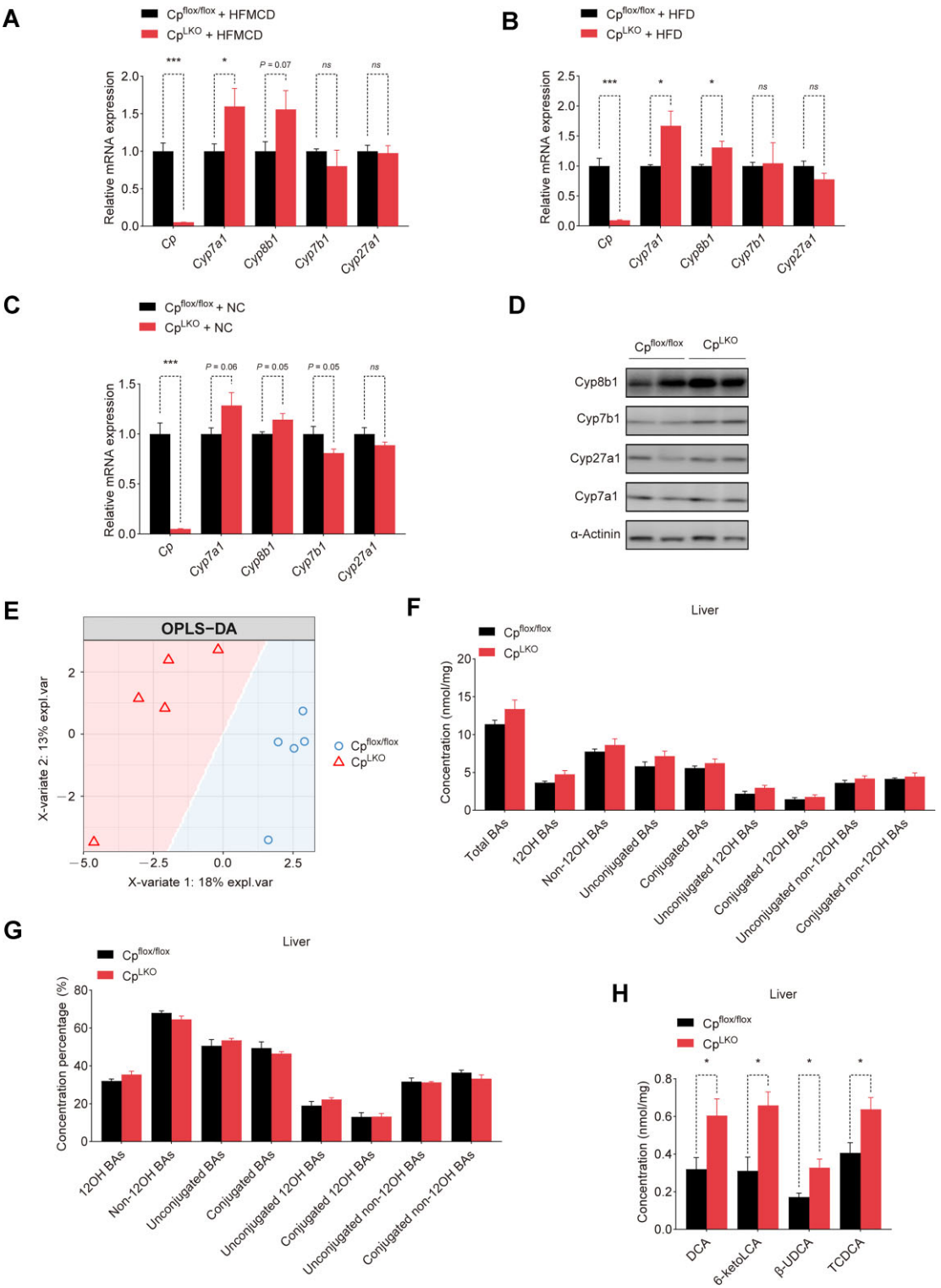

Figure 6 Hepatic Cp deficiency leads to alterations in hepatic BA biosynthesis and composition. (**A**–**C**) qRT-PCR analysis of BA synthesis-related genes in the livers from Cp^{LKO} and $Cp^{flox/flox}$ mice fed HFMCD for 8 weeks ($n = 5$/group), HFD for 12 weeks ($n = 5$/group), or NC diet for 12 weeks ($n = 6$/group). (**D**) Immunoblot analysis of BA synthesis-related liver enzymes in the livers from Cp^{LKO} and $Cp^{flox/flox}$ mice with HFD feeding. (**E**–**H**) $Cp^{flox/flox}$ and Cp^{LKO} mice were fed NC ($n = 5$/group). (**E**) OPLS-DA score plot of hepatic BA profiles. (**F** and **G**) Concentration (**F**) and concentration percentage (**G**) of hepatic BA groups. (**H**) Altered hepatic BA species. The results are presented as mean ± SEM. $^*P < 0.05$, $^{***}P < 0.001$. *ns* denotes non-significant. Concentrations of conjugated 12OH BAs and 6-ketoLCA in the livers were analyzed by Mann–Whitney *U* test; other data were analyzed by two-tailed, unpaired Student's *t*-test or with Welch correction.

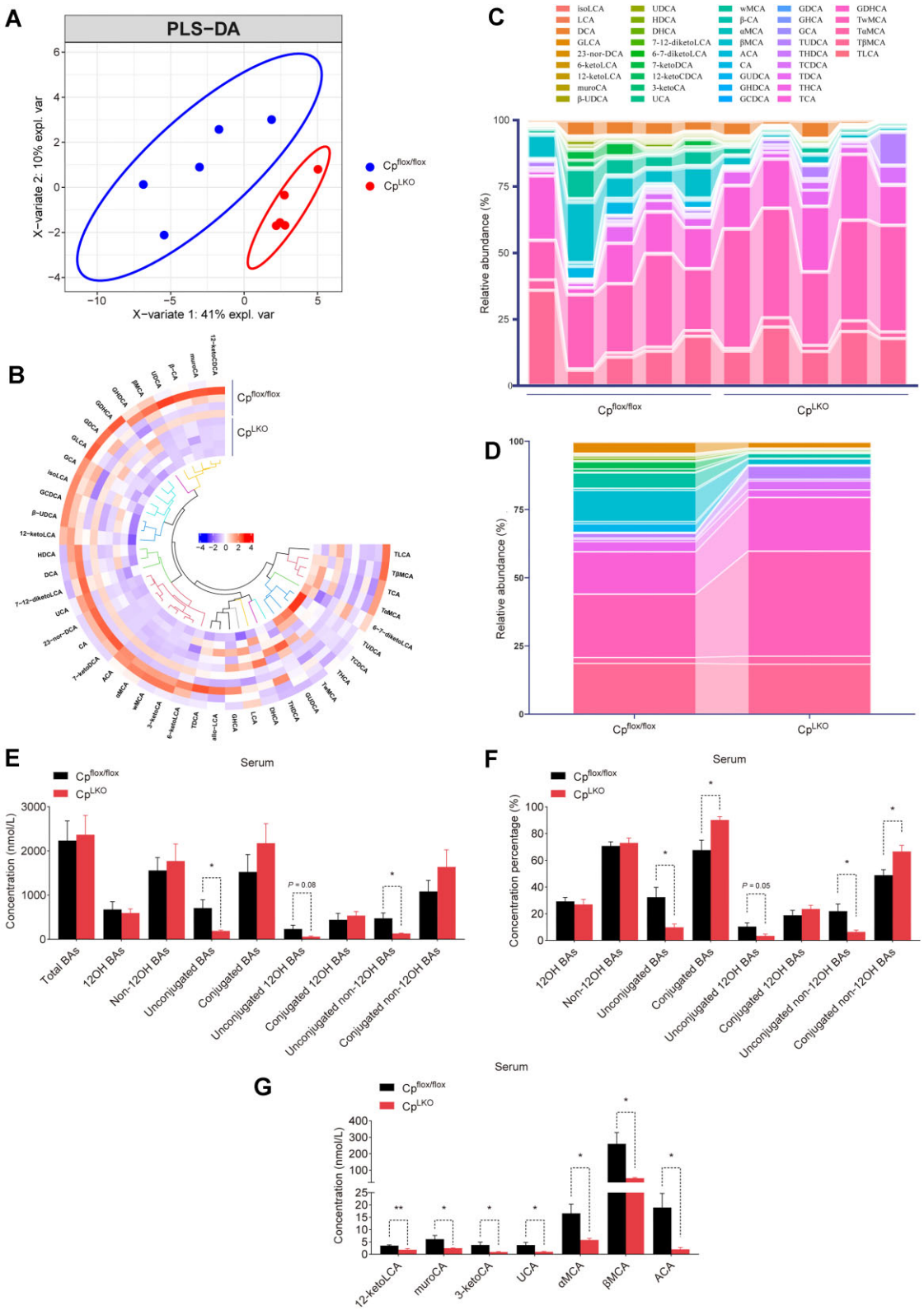

Figure 7 Hepatic-specific knockout of Cp remodels serum BA profiles. $Cp^{flox/flox}$ and Cp^{LKO} mice were fed NC ($n = 5$/group). (**A** and **B**) PLS-DA plot (**A**) and heatmap (**B**) of serum BA profiles. (**C** and **D**) Relative abundance of each BA in each sample (**C**) or each group (**D**). (**E** and **F**) Concentration (**E**) and concentration percentage (**F**) of serum BA groups. (**G**) Altered serum BA species. The results are presented as mean ± SEM. $^*P < 0.05$, $^{**}P < 0.01$. Concentrations of 12-ketoLCA were analyzed by Mann–Whitney *U* test; other data were analyzed by two-tailed, unpaired Student's *t*-test or with Welch correction.

effectively restore hepatic copper levels to the normal physiological range and activate AMPK to promote FAO (Xie et al., 2022). Here, we consistently observed a reduction in lipid accumulation upon Cp knockout in a mouse model of NASH, which was achieved through the promotion of FAO. Additionally, we found that Cp knockout upregulated the expression of liver enzymes related to BA synthesis, i.e. CYPs, a large heme-containing enzyme superfamily with multiple isoforms and subtypes. These enzymes play crucial roles in the metabolism of steroids, fatty acids, and xenobiotics (such as drugs and toxins) in mammals, in the clearance of various compounds, and in the synthesis and breakdown of hormones. Studies have shown that copper exposure can decrease the expression and activity of CYPs in the rat liver (Tang et al., 2018). Copper deficiency has also been reported to have adverse effects on production of NADPH-dependent reactive oxygen species (ROS) by CYPs in rat liver microsomes, leading to lipid peroxidation (Hammermueller et al., 1987). Copper deficiency-induced lipid peroxidation may be associated with observed iron accumulation. Therefore, the upregulation of liver enzymes involved in BA synthesis upon Cp knockout may be linked to the restoration of normal copper and iron metabolism. This correlation definitely warrants further investigation. Furthermore, the upregulated expression of BA synthesis-related liver enzymes also promotes the conversion of cholesterol into BAs in the liver. These results suggest that Cp knockout may exert therapeutic effects on fatty liver by increasing BA biosynthesis and fatty acid oxidation.

Recent studies have shown that the presence of Cp is closely associated with factors such as inflammation and hyperlipidemia (Ehrenwald et al., 1994; Ehrenwald and Fox, 1996; Mukhopadhyay et al., 1996; Fox et al., 2000). Under these conditions, Cp may interact with the surface of endothelial cells or smooth muscle cells in blood vessels. Additionally, pathogenic factors such as ROS can attack Cp, leading to structural damage and the release of free copper ions (Cu^{2+}). Subsequently, free Cu^{2+} can cause oxidation of low-density lipoprotein (LDL) in the blood, resulting in the formation of oxidized LDL, which enters endothelial cells and stimulates the production of inflammatory factors and ROS, causing more severe vascular damage and ultimately leading to cardiovascular diseases. Therefore, the deletion of Cp alleviates the inflammatory levels in NASH models, possibly by reducing oxidative stress caused by decreased Cu^{2+} levels in the blood. As mentioned earlier, OCA carries the risk of increasing LDL, TG, and TC levels in patients (Siddiqui et al., 2020), which has led to delays in obtaining NASH indication approval. Knocking out Cp can reduce serum TC and TG levels and Cp-mediated oxidation of LDL. Therefore, Cp ablation may reduce the risks associated with the direct use of BA analogs. Furthermore, Cp knockout can also lower the levels of 12OH BAs in the serum. Recent research has demonstrated that 12OH BAs can activate the TGR5 receptor on hepatic stellate cells (HSCs), leading to HSC proliferation and liver fibrosis (Xie et al., 2021). Thus, targeting Cp in the liver could potentially reduce the content of 12OH BAs in the serum, thereby preventing or alleviating liver fibrosis.

In conclusion, the findings of this study demonstrate a significant correlation between the advancement of NASH and elevated levels of hepatic Cp in both humans and mice. The elimination of Cp leads to alterations in the BA composition in the liver and serum of mice, specifically reducing the levels of 12OH BAs in the serum, and ultimately mitigates the symptoms of NASH. Consequently, this intervention can effectively impede the progression of NASH.

Materials and methods

Human samples

The program was approved by the Ethics Committee of the Sixth People's Hospital affiliated with Shanghai Jiao Tong University School of Medicine and registered in the Chinese Clinical Trial Registry (trial registration number: ChiCTR2100048122). Liver samples were obtained from 14 healthy individuals, 17 NAFL patients, and 12 NASH patients. All study participants signed informed consent forms for the use of clinical specimens in this research. The gender, age, and steatosis level (%) of each individual are provided in Supplementary Table S1.

Mouse models

The animal experiments were approved by the Ministry of Science and Technology and conducted in accordance with the Regulations of Animal Experimentation Management Legislation in China and the guidelines provided. The mice were housed under specific pathogen-free (SPF) conditions in a controlled facility, and they had *ad libitum* access to standard feed (SLACOM) and water or the specific diets as indicated (temperature 20°C–22°C, humidity 45% ± 5%, 12-h light/dark cycle). Male C57BL/6J mice (5–6 weeks old; SPF grade) were obtained from GemPharmatech. A mouse NASH model was established by feeding male C57BL/6J mice aged 6–8 weeks with HFD (60% calories from fat, 20% calories from protein, 20% calories from carbohydrates; Research Diets, D12492) or HFMCD (60% calories from fat with low methionine and no choline; Research Diets, A06071302) for 8 weeks. The liver-specific Cp knockout (Cp^{LKO}) mice were generated as described before (Xie et al., 2022). Cp^{LKO} mice and their control littermates ($Cp^{flox/flox}$) aged 6–8 weeks were fed HFD or HFMCD for 8 weeks. The mouse NAFL model was established by feeding male C57BL/6J, Cp^{LKO}, and $Cp^{flox/flox}$ mice aged 6–8 weeks with HFD for 12 weeks. At the end of the experiment, the mice were euthanized, and their livers were weighed, fixed in 4% paraformaldehyde, or frozen in liquid nitrogen.

Measurements of plasma and liver parameters

After being incubated at room temperature for 2 h, whole blood samples from mice were centrifuged at 3000 rpm at 4°C for 15 min to isolate the supernatant for further aliquoting or testing. The levels of ALT and AST in the serum were determined using commercial reagent kits (Nanjing Jiancheng, C009-1-1, C010-1-1) according to manufacturer's instructions. The serum TG, TC, NEFA, and hepatic NEFA levels were determined using

commercial reagent kits for TG (Nanjing Jiancheng, A110-1-1), TC (Elabscience, E-BC-K109-M), and NFEA (Nanjing Jiancheng, A042-2-1), respectively, following the manufacturer's instructions.

Histopathologic analysis

Liver tissues were fixed in 4% paraformaldehyde, embedded in paraffin, and cut into 5-μm-thick sections. The severity of hepatic steatosis, hepatocyte ballooning, and lobular inflammation was assessed by two independent pathologists, and the average scores for NAS were determined. Steatosis was scored on a scale of 0–3. Hepatocyte ballooning was scored on a scale of 0–2. Lobular inflammation was scored on a scale of 0–3 based on the number of inflammatory foci observed under a 20× magnification. The corresponding positive staining areas were quantified using ImageJ software, and the results were expressed as the percentage of positive staining area relative to the total area.

IHC analysis

Liver tissue embedded in paraffin was processed for deparaffinization and rehydration. The tissue sections were then treated with 10 mM citrate buffer (pH 6.0) and subjected to antigen retrieval using microwave heating for 3 min. Subsequently, the sections were incubated with 3% hydrogen peroxide solution at room temperature for 20 min to block endogenous enzymes. Blocking was carried out using serum from the same source as the secondary antibody, incubating at 37°C for 30 min. The sections were then incubated overnight at 4°C with an anti-Tnfα antibody (Bioss, bs-10802R) diluted to 1:500 in the serum corresponding to the blocking solution. On the following day, the sections were incubated with an HRP-conjugated goat anti-rabbit IgG secondary antibody, diluted to 1:2000, at room temperature for 1 h. Subsequently, the sections were processed using the DAB Peroxidase Substrate Kit (MXB Biotechnologies, DAB-4033) and stained with hematoxylin. The stained sections were imaged and scanned using a 3D digital slide scanner (3D HISTECH) and analyzed using ImageJ software.

ELISA

According to the manufacturer's instructions, the concentrations of Il1β and Tnfα in the serum were measured using mouse ELISA kits (Abclonal, RK00006, RK00027). The absorbance was measured at a wavelength of 450 nm using an ELISA reader (Molecular Devices, SpectraMax i3x).

qRT-PCR

Total RNA was isolated from hepatocytes or liver tissues using TRIzol reagent (Thermo Fisher Scientific, 15596) according to manufacturer's instructions. The quality and concentration of RNA were assessed by measuring the absorbance at 260 nm and 280 nm using a NanoDrop 2000C spectrophotometer (Thermo Fisher Scientific). cDNA was synthesized from 1 μg of RNA using the ABScript III RT Master Mix (ABclonal, RK20428). The primers for qRT-PCR analysis were synthesized by Biosun Biotech. Subsequently, qRT-PCR was performed using the Universal SYBR Green Fast qRT-PCR Mix (ABclonal, RK21203) on a LightCycler 480 II (Roche Life Science). The expression levels of the target genes were normalized to the reference gene level (Actb) and analyzed using the ΔΔCT method. The primer sequences used for qRT-PCR are listed in Supplementary Table S2.

Isolation and culture of primary hepatocytes

Male mice aged 6–8 weeks were anesthetized and perfused through the portal vein at a rate of 8 ml/min with perfusion buffer and collagenase-I (0.5 mg/ml; Worthington Biochemical, LS004196) at 37°C. After digestion, the liver was excised, minced, filtered through a 70-μm cell strainer (Thermo Fisher Scientific), and centrifuged at 400 rpm for 3 min at 4°C. The cells were then resuspended in 50% Percoll solution (GE Healthcare Life Sciences, 17-0891-01) and centrifuged at 700× *g* for 10 min at 4°C to purify the hepatocytes. The purified hepatocytes were resuspended in Medium 199 (Sigma) supplemented with 10% fetal bovine serum (Gibco) and 1% penicillin/streptomycin (Gibco, 15140-122) and plated at the specified density in culture dishes. To establish an *in vitro* model of NASH in hepatocytes, 0.2 mM PA (Sigma-Aldrich) was added to the medium containing 0.5% bovine serum albumin (BSA), and the cells were cultured for 12–36 h. Hepatocytes were cultured at 37°C with 5% CO_2 under a humidified atmosphere in a cell incubator.

Isolation of HPCs and NPCs

HPCs and NPCs were primarily extracted from male mice that were fed HFMCD for 8 weeks. Firstly, the portal vein was exposed, and the liver was perfused with a perfusion buffer to remove blood. Subsequently, a collagenase-containing perfusion solution was used to digest the liver, after which the digested liver tissue was excised and dispersed to obtain cells. The cell suspension was then filtered through a 100-μm cell strainer and centrifugated at 50× *g* for 5 min to pellet HPCs, while the supernatant was collected to obtain NPCs. HPCs were subsequently purified by resuspending the pellet and centrifuging it several times. Next, the supernatant was subjected to centrifugation at 100× *g* for 5 min to eliminate HPCs and red blood cells that had settled at the bottom. The collected supernatant was then centrifuged at 300× *g* for 5 min to retain the supernatant, after which it was further centrifuged at 650× *g* for 7 min to obtain NPCs. The collected HPCs and NPCs were then subjected to qRT-PCR analysis.

Nile red staining

Primary hepatocytes were washed with phosphate-buffered saline (PBS) and fixed with 4% paraformaldehyde at room temperature for 30 min. Subsequently, the cells were incubated with 1 μg/ml Nile Red (Sigma-Aldrich, 72485) for 10 min at 37°C. Afterward, the cells were washed three times with PBS. Images were captured using an Olympus spinning disk confocal super-resolution microscope (IXplore SpinSR10).

Bioinformatics analysis

Differential gene expression data were obtained from the GEO database. The datasets GSE164084, GSE167523, GSE89063, GSE89632, and GSE115193 related to NASH were downloaded. For transcriptomic analysis, the raw data of RNA-seq on mouse liver tissues were obtained from our previous study (Xie et al., 2022). The data were imported into R (version 4.1.3), and PCA analysis was performed using the 'FactoMineR' package to identify outlier samples. Differential gene expression analysis was conducted using the 'DEseq2' package, with a gene selection threshold of $P < 0.05$ and $|\log_2(\text{fold change})| > 1$. The 'ReactomePA' package was used for enrichment analysis of the Reactome database to study the biological characteristics of these genes. For the analysis of BAs, OPLS-DA and PLS-DA were performed using the 'mixOmics' package in R to assess whether the two groups could be distinguished. The relevant code for this study is available at https://github.com/Eliauk-clumsy/Analysis.git.

Immunoblotting

Liver or hepatocyte samples were lysed in RIPA lysis buffer (Beyotime, P0013B) containing protease inhibitor (ApexBio Technology, K1008) and phosphatase inhibitor (ApexBio Technology, K1015) and incubated on a rotating shaker at 4°C for 15 min. The lysates were then centrifuged at 3000× *g* for 10 min to remove debris. The supernatant was collected, and the protein concentration was determined using a BCA Protein Assay Kit (Thermo, 23225). The samples were diluted to a concentration of 5 μg/μl with loading buffer and denatured by boiling at 100°C for 5 min. After sodium dodecylsulfate–polyacrylamide gel electrophoresis (SDS–PAGE), the proteins were transferred onto a polyvinylidene fluoride membrane (pore size 0.22 μm; Millipore). The membrane was blocked in Tris-buffered saline with 0.1% Tween-20 (TBST) containing 5% skim milk at room temperature for 1 h. Subsequently, the membrane was incubated overnight at 4°C with primary antibodies. The next day, the membrane was washed three times with TBST for 10 min each, followed by incubation with secondary antibodies at room temperature for 1 h. After washing the membrane three times with TBST for 10 min each, the protein bands were visualized using an ECL detection reagent (Tanon, 180-501). α-Actinin or β-Actin served as a loading control. The relative intensities of the bands were quantified using ImageJ software (NIH). Serum samples were diluted with loading buffer. After SDS–PAGE, the proteins were transferred onto a polyvinylidene fluoride membrane. Ponceau S was used to stain membrane as a loading control. The antibodies used in this study were: rabbit monoclonal anti-α-Actinin antibody, 1:2000 (Cell Signaling Technology, 6487); rabbit polyclonal anti-Ceruloplasmin antibody, 1:1000 (Thermo Fisher Scientific, PA5-14225); mouse polyclonal anti-Cyp7a1 antibody, 1:1000 (Santa Cruz, sc-518007); mouse polyclonal anti-Cyp8b1 antibody, 1:1000 (Santa Cruz, sc-101387); rabbit polyclonal anti-Cyp7b1 antibody, 1:1000 (Abclonal, A17872); rabbit monoclonal anti-Cyp27a1 antibody, 1:1000 (Abclonal, A23250); rabbit polyclonal anti-Cpt1α antibody, 1:1000 (Proteintech, 15184-1-AP); rabbit monoclonal anti-Pparα antibody, 1:1000 (Proteintech, 66826-1-Ig); rabbit polyclonal anti-β-Actin antibody, 1:1000 (Proteintech, 20536-1-AP).

BA measurement

The BA profiles in the serum and liver samples from the mice fed normal chow diet were measured using UPLC–MS/MS (ACQUITYUPLC–XevoTQ-S; Waters), performed at the Center for Translational Medicine of the Sixth People's Hospital affiliated with the Shanghai Jiao Tong University School of Medicine. The raw data were quantified and analyzed using MassLynx software (v4.1; Waters). In the liver samples, a total of 46 different BAs were detected, while in the serum samples, a total of 42 different bile acids were detected. The total BA level represents the sum of all quantified BAs in the samples.

Quantification and statistical analysis

The statistical analysis was performed using GraphPad Prism 9.0 software (GraphPad Software). The data were presented as mean ± standard error of the mean (SEM). Before conducting the significance analysis, the normality of the data was assessed using the Shapiro–Wilk test and Kolmogorov–Smirnov test. For data that followed a normal distribution and exhibited homogeneity of variance, a two-tailed, unpaired Student's *t*-test was used to compare the differences between two groups. For skewed data, the Mann–Whitney *U* test was employed for statistical analysis. Differences between three or more groups were evaluated either through one-way ANOVA for normally distributed data or the Kruskal Wallis test otherwise. The relationship between two quantitative variables was evaluated using linear regression analysis and Pearson's or Spearman correlation coefficient (*r*) when appropriate. A *P*-value <0.05 was considered statistically significant; $^*P < 0.05$, $^{**}P < 0.01$, and $^{***}P < 0.001$. Mouse body weight measurements and histological analysis were performed and analyzed in a blinded manner. The sample size for each experiment was determined based on previous studies and preliminary results conducted in our laboratory (Chen et al., 2021; Xie et al., 2022).

Supplementary material

Supplementary material is available at *Journal of Molecular Cell Biology* online.

Acknowledgements

We sincerely thank Dr Jian Li (Shanghai Sixth People's Hospital), Dr Shuang Liu (Tianjin Medical University), as well as Dr Yunqing Gu, Dr Xiaojiao Zheng, Ms Xue Peng, Mr Yanyu Zhai, and Ms Yao Zhang at Shanghai Sixth People's Hospital for technical assistance.

Funding

This work was supported by grants to S.C. from the National Natural Science Foundation of China (82170863), Shanghai Rising-Star Program (21QA1407000), the Lingang

Laboratory Grant (LG-QS-202205-06), the Innovative Research Team of High-level Local Universities in Shanghai (SHSMU-ZDCX20212501), and Shanghai Sixth People's Hospital (ynyq202103). This work was also supported by grants to J.L. from the National Key R&D Program of China (2021YFA0804800 and 2018YFA0800600), Shanghai Municipal Commission of Science and Technology (20410713200 and 21S11909000), the National Facility for Translational Medicine (TMSK-2020-102), the 'Shuguang Program' supported by Shanghai Education Development Foundation and Shanghai Municipal Education Commission (20SG10), and Shanghai Sixth People's Hospital (ynjq202102).

Conflict of interest: none declared.

References

Aigner, E., Strasser, M., Haufe, H., et al. (2010). A role for low hepatic copper concentrations in nonalcoholic fatty liver disease. Am. J. Gastroenterol. *105*, 1978–1985.

Blades, B., Ayton, S., Hung, Y.H., et al. (2021). Copper and lipid metabolism: a reciprocal relationship. Biochim. Biophys. Acta Gen. Subj. *1865*, 129979.

Brandl, K., Hartmann, P., Jih, L.J., et al. (2018). Dysregulation of serum bile acids and FGF19 in alcoholic hepatitis. J. Hepatol. *69*, 396–405.

Chen, S., Liu, X., Peng, C., et al. (2021). The phytochemical hyperforin triggers thermogenesis in adipose tissue via a Dlat–AMPK signaling axis to curb obesity. Cell Metab. *33*, 565–580.e7.

Chiang, J.Y. (2004). Regulation of bile acid synthesis: pathways, nuclear receptors, and mechanisms. J. Hepatol. *40*, 539–551.

Cortes, V., and Eckel, R.H. (2022). Insulin and bile acids in cholesterol homeostasis: new players in diabetes-associated atherosclerosis. Circulation *145*, 983–986.

de Aguiar Vallim, T.Q., Tarling, E.J., and Edwards, P.A. (2013). Pleiotropic roles of bile acids in metabolism. Cell Metab. *17*, 657–669.

Ehrenwald, E., Chisolm, G.M., and Fox, P.L. (1994). Intact human ceruloplasmin oxidatively modifies low density lipoprotein. J. Clin. Invest. *93*, 1493–1501.

Ehrenwald, E., and Fox, P.L. (1996). Role of endogenous ceruloplasmin in low density lipoprotein oxidation by human U937 monocytic cells. J. Clin. Invest. *97*, 884–890.

Engstrom, G., Stavenow, L., Hedblad, B., et al. (2003). Inflammation-sensitive plasma proteins, diabetes, and mortality and incidence of myocardial infarction and stroke: a population-based study. Diabetes *52*, 442–447.

Eslam, M., Alvani, R., and Shiha, G. (2019). Obeticholic acid: towards first approval for NASH. Lancet *394*, 2131–2133.

Fiorucci, S., Distrutti, E., Carino, A., et al. (2021). Bile acids and their receptors in metabolic disorders. Prog. Lipid Res. *82*, 101094.

Flemming, A. (2023). Copper boosts pro-inflammatory state of macrophages. Nat. Rev. Immunol. *23*, 344.

Fox, P.L., Mazumder, B., Ehrenwald, E., et al. (2000). Ceruloplasmin and cardiovascular disease. Free Radic. Biol. Med. *28*, 1735–1744.

Goh, G.B., and McCullough, A.J. (2016). Natural history of nonalcoholic fatty liver disease. Dig. Dis. Sci. *61*, 1226–1233.

Gu, L., Zhu, Y., Watari, K., et al. (2023). Fructose-1,6-bisphosphatase is a nonenzymatic safety valve that curtails AKT activation to prevent insulin hyperresponsiveness. Cell Metab. *35*, 1009–1021. e9.

Gulec, S., and Collins, J.F. (2014). Molecular mediators governing iron–copper interactions. Annu. Rev. Nutr. *34*, 95–116.

Hammermueller, J.D., Bray, T.M., and Bettger, W.J. (1987). Effect of zinc and copper deficiency on microsomal NADPH-dependent active oxygen generation in rat lung and liver. J. Nutr. *117*, 894–901.

Harder, N.H.O., Lee, H.P., Flood, V.J., et al. (2022). Fatty acid uptake in liver hepatocytes induces relocalization and sequestration of intracellular copper. Front. Mol. Biosci. *9*, 863296.

Harris, E.D. (2000). Cellular copper transport and metabolism. Annu. Rev. Nutr. *20*, 291–310.

Harrison, S.A., Allen, A.M., Dubourg, J., et al. (2023). Challenges and opportunities in NASH drug development. Nat. Med. *29*, 562–573.

Hubscher, S.G. (2003). Iron overload, inflammation and fibrosis in genetic haemochromatosis. J. Hepatol. *38*, 521–525.

Huby, T., and Gautier, E.L. (2022). Immune cell-mediated features of non-alcoholic steatohepatitis. Nat. Rev. Immunol. *22*, 429–443.

Jiao, T.Y., Ma, Y.D., Guo, X.Z., et al. (2022). Bile acid and receptors: biology and drug discovery for nonalcoholic fatty liver disease. Acta Pharmacol. Sin. *43*, 1103–1119.

Kew, M.C. (2000). Serum aminotransferase concentration as evidence of hepatocellular damage. Lancet *355*, 591–592.

Kim, C.H., Park, J.Y., Kim, J.Y., et al. (2002). Elevated serum ceruloplasmin levels in subjects with metabolic syndrome: a population-based study. Metabolism *51*, 838–842.

Kim, T.H., Hong, D.G., and Yang, Y.M. (2021). Hepatokines and non-alcoholic fatty liver disease: linking liver pathophysiology to metabolism. Biomedicines *9*, 1903.

Linder, M.C. (2016). Ceruloplasmin and other copper binding components of blood plasma and their functions: an update. Metallomics *8*, 887–905.

Loomba, R., Friedman, S.L., and Shulman, G.I. (2021). Mechanisms and disease consequences of nonalcoholic fatty liver disease. Cell *184*, 2537–2564.

Mänttäri, M., Manninen, V., Huttunen, J., et al. (1994). Serum ferritin and ceruloplasmin as coronary risk factors. Eur. Heart J. *15*, 1599–1603.

Marra, F., and Svegliati-Baroni, G. (2018). Lipotoxicity and the gut–liver axis in NASH pathogenesis. J. Hepatol. *68*, 280–295.

Masoodi, M., Gastaldelli, A., Hyotylainen, T., et al. (2021). Metabolomics and lipidomics in NAFLD: biomarkers and non-invasive diagnostic tests. Nat. Rev. Gastroenterol. Hepatol. *18*, 835–856.

Meunier, B., Visser, S.P., and Shaik, S. (2004). Mechanism of oxidation reactions catalyzed by cytochrome p450 enzymes. Chem. Rev. *104*, 3947–3980.

Michelotti, G.A., Machado, M.V., and Diehl, A.M. (2013). NAFLD, NASH and liver cancer. Nat. Rev. Gastroenterol. Hepatol. *10*, 656–665.

Montgomery, M.K., Bayliss, J., Nie, S., et al. (2022). Deep proteomic profiling unveils arylsulfatase A as a non-alcoholic steatohepatitis inducible hepatokine and regulator of glycemic control. Nat. Commun. *13*, 1259.

Mukhopadhyay, C.K., Ehrenwald, E., and Fox, P.L. (1996). Ceruloplasmin enhances smooth muscle cell- and endothelial cell-mediated low density lipoprotein oxidation by a superoxide-dependent mechanism. J. Biol. Chem. *271*, 14773–14778.

Pikuleva, I.A. (2006). Cytochrome P450s and cholesterol homeostasis. Pharmacol. Ther. *112*, 761–773.

Preziosi, M.E., Singh, S., Valore, E.V., et al. (2017). Mice lacking liver-specific β-catenin develop steatohepatitis and fibrosis after iron overload. J. Hepatol. *67*, 360–369.

Roeser, H.P., Lee, G.R., Nacht, S., et al. (1970). The role of ceruloplasmin in iron metabolism. J. Clin. Invest. *49*, 2408–2417.

Samygina, V.R., Sokolov, A.V., Bourenkov, G., et al. (2017). Rat ceruloplasmin: a new labile copper binding site and zinc/copper mosaic. Metallomics *9*, 1828–1838.

Sheka, A.C., Adeyi, O., Thompson, J., et al. (2020). Nonalcoholic steatohepatitis: a review. JAMA *323*, 1175–1183.

Siddiqui, M.S., Van Natta, M.L., Connelly, M.A., et al. (2020). Impact of obeticholic acid on the lipoprotein profile in patients with non-alcoholic steatohepatitis. J. Hepatol. *72*, 25–33.

Sorbi, D., Boynton, J., and Lindor, K.D. (1999). The ratio of aspartate aminotransferase to alanine aminotransferase: potential value in differentiating nonalcoholic steatohepatitis from alcoholic liver disease. Am. J. Gastroenterol. *94*, 1018–1022.

Stefan, N., Schick, F., Birkenfeld, A.L., et al. (2023). The role of hepatokines in NAFLD. Cell Metab. *35*, 236–252.

Tang, H., Xu, M., Shi, F., et al. (2018). Effects and mechanism of nano-copper exposure on hepatic cytochrome P450 enzymes in rats. Int. J. Mol. Sci. *19*, 2140.

Tang, Z., Gasperkova, D., Xu, J., et al. (2000). Copper deficiency induces hepatic fatty acid synthase gene transcription in rats by increasing the nuclear content of mature sterol regulatory element binding protein 1. J. Nutr. *130*, 2915–2921.

Tveter, K.M., Mezhibovsky, E., Wu, Y., et al. (2023). Bile acid metabolism and signaling: emerging pharmacological targets of dietary polyphenols. Pharmacol. Ther. *248*, 108457.

Vasilyev, V.B. (2010). Interactions of caeruloplasmin with other proteins participating in inflammation. Biochem. Soc. Trans. *38*, 947–951.

Wahlstrom, A., Sayin, S.I., Marschall, H.U., et al. (2016). Intestinal crosstalk between bile acids and microbiota and its impact on host metabolism. Cell Metab. *24*, 41–50.

Xie, G., Jiang, R., Wang, X., et al. (2021). Conjugated secondary 12α-hydroxylated bile acids promote liver fibrogenesis. EBioMedicine *66*, 103290.

Xie, L., Yuan, Y., Xu, S., et al. (2022). Downregulation of hepatic ceruloplasmin ameliorates NAFLD via SCO1–AMPK–LKB1 complex. Cell Rep. *41*, 111498.

Younossi, Z., Anstee, Q.M., Marietti, M., et al. (2018). Global burden of NAFLD and NASH: trends, predictions, risk factors and prevention. Nat. Rev. Gastroenterol. Hepatol. *15*, 11–20.

Younossi, Z.M., Koenig, A.B., Abdelatif, D., et al. (2016). Global epidemiology of nonalcoholic fatty liver disease—meta-analytic assessment of prevalence, incidence, and outcomes. Hepatology *64*, 73–84.

Younossi, Z.M., Ratziu, V., Loomba, R., et al. (2019). Obeticholic acid for the treatment of non-alcoholic steatohepatitis: interim analysis from a multicentre, randomised, placebo-controlled phase 3 trial. Lancet *394*, 2184–2196.

Zhang, P., Wang, P.X., Zhao, L.P., et al. (2018). The deubiquitinating enzyme TNFAIP3 mediates inactivation of hepatic ASK1 and ameliorates nonalcoholic steatohepatitis. Nat. Med. *24*, 84–94.

Zhou, J., Zhou, F., Wang, W., et al. (2020). Epidemiological features of NAFLD from 1999 to 2018 in China. Hepatology *71*, 1851–1864.

Received July 16, 2023. Revised September 19, 2023. Accepted September 27, 2023.